Hindawi
Geofluids
Volume 2018, Article ID 2525132, 13 pages
https://doi.org/10.1155/2018/2525132

Research Article

Impact of SO_2 on Alteration of Reservoir Rock with Ca-Deficient Conditions and Poor Buffering Capacity under a CO_2 Geologic Storage Condition

Jinyoung Park,[1,2] Byoung-Young Choi,[1] Jong Ok Jeong,[3] and Young Jae Shinn[1]

[1]*Center for CO_2 Geological Storage, Korea Institute of Geoscience and Mineral Resources (KIGAM), Daejeon 305-350, Republic of Korea*
[2]*Department of Earth Environmental Sciences, Pukyong National University, Busan 608-737, Republic of Korea*
[3]*Center for Research Facilities, Gyeongsang National University, Jinju 600-701, Republic of Korea*

Correspondence should be addressed to Byoung-Young Choi; choiby@kigam.re.kr

Received 21 September 2017; Accepted 22 January 2018; Published 15 February 2018

Academic Editor: Ferenc Molnar

The objective of this study is to evaluate the impact of SO_2-CO_2-water-rock interaction on the alteration of a reservoir rock having Ca-deficient conditions and little buffering capacity and its implication for porosity change near the injection well from a CO_2 storage pilot site, Republic of Korea. For our study, three cases of experimental and geochemical modeling were carried out (pure CO_2, 0.1% SO_2 in CO_2, and 1% SO_2 in CO_2, resp.) under realistic geologic storage conditions. Our results show that SO_2 accelerated water-rock interactions by lowering the pH. In the 1% SO_2 case, pH remained less than 2 during the experiments because of insufficient buffering capacity. Sulfate minerals were not precipitated because of an insufficient supply of Ca. Because the total volume of precipitated secondary minerals was less than that of the dissolved primary minerals, the porosity of rock increased in all cases. Chlorite largely contributed to the decrease in total rock volume although it formed only 4.8 wt.% of the rock. Our study shows that the coinjection of a certain amount of SO_2 at CO_2 storage reservoirs without carbonate and Ca-rich minerals can significantly increase the porosity by enhancing water-rock interactions. This procedure can be beneficial to CO_2 injection under some conditions.

1. Introduction

Carbon dioxide Capture and Storage (CCS) is a solution to reduce atmospheric emissions of CO_2 which are recognized as the main cause of global warming [1]. For storage, CO_2 is captured in fossil-fuel-based power plants and other industrial facilities. The flue gas from these sources contains not only CO_2 but also various impurities such as sulfur dioxide (SO_2), oxygen (O_2), nitrogen (N_2), hydrogen (H_2), and carbon monoxide (CO) [2–5]. The process of removing these impurities to obtain pure CO_2 is costly; thus, the coinjection of impurities has an advantage in that it can reduce costs significantly. However, the coinjection of impurities not only corrodes injection facilities, such as pipelines and injection wells, but also adversely affects CO_2 injectivity [2, 5, 6]. Among these impurities, coinjection of even a small amount of SO_2 extremely acidifies the groundwater due to formation of sulfuric acid, which accelerates the dissolution/precipitation of minerals in reservoir rocks [6–8].

The coinjection of SO_2 thus has the potential to significantly change the porosity and permeability of a reservoir rock which in turn affects the injectivity of fluid transport [6, 9–11]. However, to the best of our knowledge, most studies on the effect of SO_2 have been performed in rocks containing Ca-rich minerals (e.g., calcite and anorthite), easily buffering the pH [4, 6, 8, 12–16]. These studies showed that SO_2 did not largely influence the alteration of reservoir rocks because pH was quickly buffered enough to prevent significant dissolution of silicate minerals. However, because of elevated Ca concentrations from Ca-rich minerals, sulfate minerals such as anhydrate, gypsum, and alunite precipitated, which decreased the porosity and permeability of the reservoir rocks.

In this study, we collected reservoir rock samples at a CO_2 storage pilot site (Pohang Basin) in Korea [17]. Mineralogical analysis of the samples showed that the reservoir rock had few carbonate and Ca-rich minerals. We aimed to identify the effect of SO_2 on water-rock interactions in the reservoir rock having poor Ca and buffering capacity and to evaluate the change in porosity affecting the CO_2 injectivity. For this study, batch experiments were performed under realistic geologic storage conditions with various SO_2 contents. Geochemical modeling was also carried out to interpret the results of gas-water-rock interactions and calculate the change in porosity.

This study will provide information about the effect of SO_2 on the change in porosity by SO_2-water-rock interactions to other CO_2 storage sites similar to our study area having few carbonate and Ca-rich minerals.

2. Materials and Methods

2.1. Reservoir Rock Samples. In Korea, a CO_2 offshore storage pilot project has been launched in Pohang Basin in the southeastern part of the Korean peninsula (Figure 1) [17]. Pohang Basin is one of the Cenozoic sedimentary basins which formed during back-arc spreading of the East Sea in the early Miocene [18–20]. The basin is bounded by a set of NNE-trending border faults in the west and opens towards the east. During the back-arc spreading, a number of pull-apart half-grabens were produced by NNW-SSE directed dextral strike-slip and associated extensional deformation, and then a km-thick sequence of nonmarine to shallow marine sediments were deposited in the graben [20]. The sediments mostly consist of a coarse-grained fan-delta succession and an overlying fine-grained succession of hemipelagic mudstone with thin interbeds of siltstone and sandstone [21–23].

The reservoir rock of Pohang Basin is developed at depths of more than 750 m and covered with a thick mudstone cap rock (Figure 1) [20, 24]. The location of the injection in the well is sandstone layer (768–782 meters below the seafloor) overlying the mudstone cap rock [17]. For the experiments, sandstone samples in the injection layer were collected from core samples recovered during drilling of a borehole to a depth of 1 km.

The mineralogical compositions of the rock samples were determined using X-ray diffraction (XRD) (Bruker, D8 ADVANCE A25) and Scanning Electron Microscopy with an Energy-Dispersive Spectroscopy (SEM-EDS) (JEOL, JSM-7610F) at the Center for Research Facilities at Gyeongsang National University. The total surface area of the sample was analyzed using a crushed sample (grain size from 100 to 200 μm) using the Brunauer-Emmett-Teller (BET) method (Quantachrome, QUADRASORB SI) at the Korea Institute of Geoscience and Mineral Resources (KIGAM).

2.2. Experiments and Analytical Methods. The SO_2-CO_2-water-rock reaction experiments were carried out in three cases to evaluate the impact of SO_2 contents on water-rock interactions: case 1: pure CO_2; case 2: 0.1% SO_2 in pure CO_2; and case 3: 1% SO_2 in pure CO_2. The rock sample used in the experiment was crushed and sieved to a grain size ranging from 100 to 200 μm. The sieved samples were sonicated five times using an ultrasonic bath filled with ethanol for 10 minutes to remove the microparticles attached to the grain surface. They were then rinsed with distilled water and dried in an oven at 50°C for 24 hours. Then, 4 g of the dried samples was placed in a cellulose dialysis tube (Thermo, 12,000 to 14,000 Da, 21 mm diameter), and 130 ml of deoxygenated distilled water (by N_2 purging) was added in a high-pressure reactor (Parr Instrument, 5500 series) with a stirrer and dip tube. A Teflon liner was used to prevent corrosion of the reactor. The cellulose dialysis membrane allows diffusion of aqueous ions between the inner and outer solutions across the membrane but confines solid samples to the inside of the dialysis tube, thereby eliminating the loss of solid particles during fluid sampling [25, 26].

Pure CO_2 gas and mixed gases were injected using a syringe pump (TELEDYNE ISCO, 500HP), and the inside of the reactor was purged with CO_2 for 20 minutes to remove the residual gas in the distilled water and headspace. Each reaction experiment was carried out for 21 days at a condition of 50°C and 100 bar and a stirring rate of 80–100 rpm.

During the experiments, approximately 3 ml of fluid was sampled through the deep tube in a syringe on the 3rd, 7th, 15th, and 21st days to measure the pH and analyze fluid composition. Before each fluid sampling, approximately 2 ml of fluid was discarded to eliminate unreacted fluid in the sampling port line.

After sampling, the pH of the sampled fluid was immediately measured using a micro pH probe (Thermo, 8103BNUWP). The fluid samples were then filtered using a 0.2 μm syringe filter (ADVANTEC) and diluted 10 times for chemical analysis. The aliquot of the diluted fluid sample was analyzed for sulfate concentration using a spectrophotometer (Hach, DR1900). Another aliquot of diluted fluid sample was acidified to HNO_3 for analysis of cations using Inductively Coupled Plasma-Optical Emission Spectroscopy (ICP-OES) (Perkin Elmer, 8300DV) at the KIGAM. The solid samples were collected at the end of reaction experiments, rinsed with distilled water, and then dried at 50°C in an oven. For the dried solid samples, XRD and SEM-EDS analyses were performed to identify mineralogical change after the experiments.

2.3. Geochemical Modeling. Geochemical modeling was performed using PHREEQC (version 3) [27] using the Lawrence Livermore National Laboratory (LLNL) database to interpret the experimental results. Dissolution/precipitation reactions in the kinetic model were calculated by using the following rate law equation [28]:

$$r = Ak\left[1 - \frac{Q}{K}\right], \tag{1}$$

where r is the reaction rate (mol/s), k is the rate constant (mol/cm^2·s), A is the reactive surface area of the mineral (cm^2), Q is the activity product, and K is the equilibrium

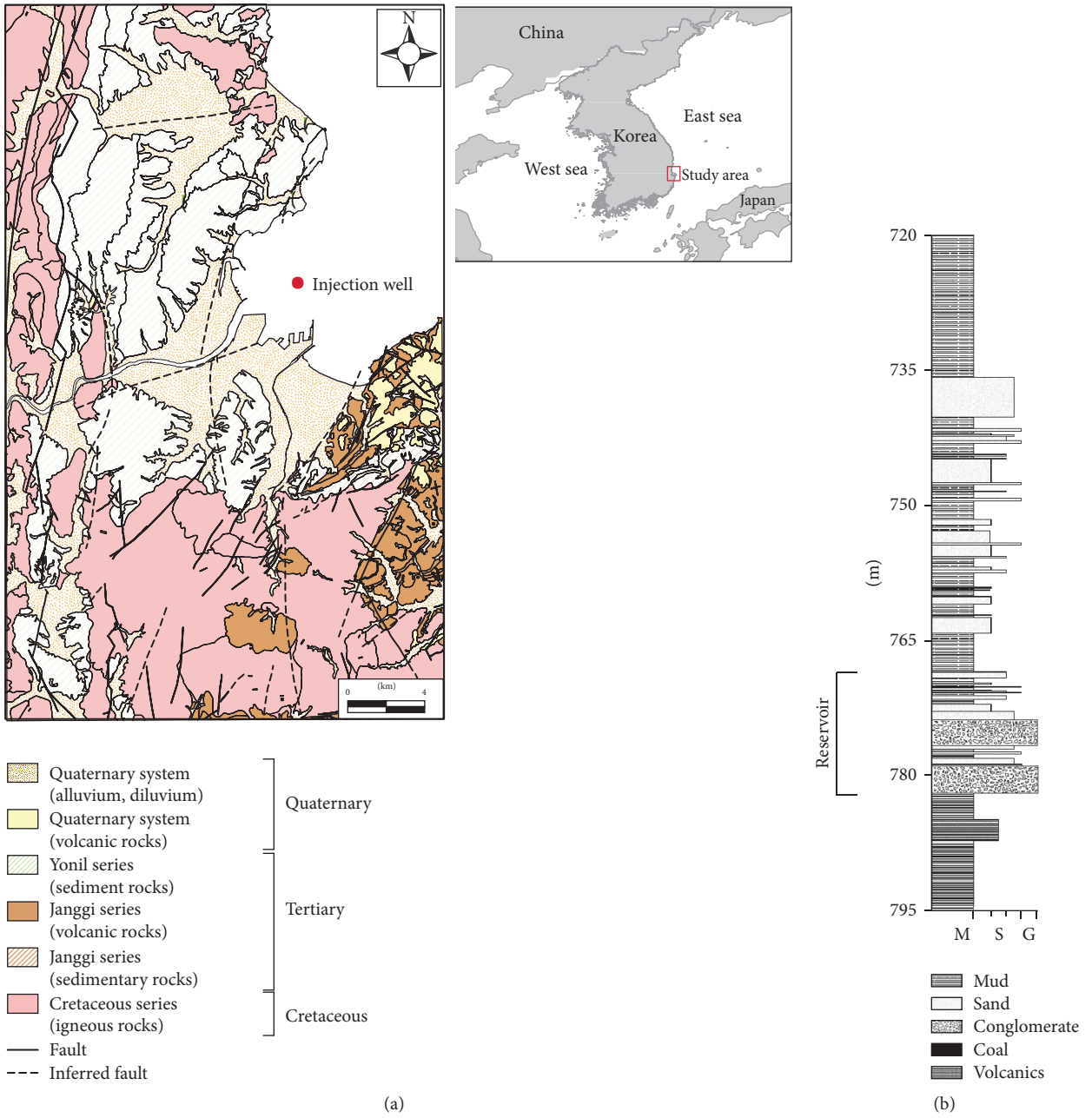

FIGURE 1: (a) A geologic map of the study area and location of the injection well in the Pohang Basin (modified from Lee et al. [24]) and (b) the sedimentary log of the injection well core (modified from Choi et al. [17]).

constant (saturation index (SI) = $\log Q/K$). The rate constant was calculated using the Arrhenius equation:

$$k = k_{25} \exp\left[\frac{-E_a}{R}\left(\frac{1}{T} - \frac{1}{298.15}\right)\right], \quad (2)$$

where k_{25} is the rate constant at 25°C, E_a is the activation energy, R is the gas constant, and T is the absolute temperature. The kinetics of the mineral reaction are pH-dependent: therefore, mineral reaction rate is calculated by individual reaction mechanisms (acid, neutral, and base mechanisms) depending on pH, as in the following equations:

$$\begin{aligned} r = s\Bigg[&k_a \exp\left[\frac{-E_a}{R}\left(\frac{1}{T} - \frac{1}{298.15}\right)\right] a_{H^+}^{n_a}\left[1 - \left(\frac{Q}{K}\right)\right] \\ &+ k_n \exp\left[\frac{-E_n}{R}\left(\frac{1}{T} - \frac{1}{298.15}\right)\right]\left[1 - \left(\frac{Q}{K}\right)\right] \\ &+ k_b \exp\left[\frac{-E_b}{R}\left(\frac{1}{T} - \frac{1}{298.15}\right)\right] a_{H^+}^{n_b}\left[1 - \left(\frac{Q}{K}\right)\right]\Bigg], \end{aligned} \quad (3)$$

where a, n, and b represent the acid, neutral, and base mechanisms, respectively. E is the activation energy, k is

Table 1: Mineral composition of the sandstone sample using XRD analysis.

Mineral	Weight%
Quartz	44.6
Plagioclase	26.4
K-feldspar	19.6
Chlorite	4.8
Kaolinite	4.3
Illite	0.3

the rate constant, R is the gas constant, T is the absolute temperature, Q is the activity product, K is the equilibrium constant, a is activity of the species, n is the power constant, and s is the specific reactive surface area per gram of mineral.

In the model, the primary minerals were defined based on the XRD and SEM-EDS analyses. From XRD analysis, the rock samples were composed of predominantly silicate minerals (44.6% quartz, 26.4% plagioclase, and 19.6% K-feldspar) and clay minerals (4.8% chlorite, 4.3% illite, and 0.3% kaolinite) (Table 1). In SEM-EDS analysis, carbonate and Ca-rich minerals were not observed.

The concentration of each mineral was calculated by mineral weight percent for 4 g of rock. In the case of a solid solution, plagioclase was represented as albite, but a small quantity of anorthite was added for matching the Ca concentration measured in the reaction experiment. Chlorite was represented as daphnite-14A (Fe end member) and clinochlore-14A (Mg end member) at a ratio of 2 : 1 based on the results of the SEM-EDS analysis.

The surface area of each mineral was calculated by dividing the BET surface area based on the mineral weight percent. However, the actual geochemical reaction occurs only at the reactive surface area. The reaction is up to three orders of magnitude less than the total surface area measured by BET or geometric methods because of surface coatings [29]. For this reason, surface area was a parameter with great uncertainty in the geochemical modeling. In this study, the surface area was modified by trial and error within 10–100 times to match the experimental results of other studies [12, 30].

Kinetic parameters of minerals were those of Palandri and Kharaka [31] except for pyrite (Table 2). Kinetic parameters of pyrite were those of Xu et al. [32].

Saturation index (SI) indicates the equilibrium condition of a solution with respect to a mineral [22]:

$$\mathrm{SI} = \log_{10}\left(\frac{\mathrm{IAP}}{K}\right). \quad (4)$$

SI = 0: mineral is in equilibrium with solution.

SI < 0: mineral is undersaturated (dissolution).

SI > 0: mineral is oversaturated (precipitation).

IAP is the ion activity product and K is the thermodynamic equilibrium constant for the reaction.

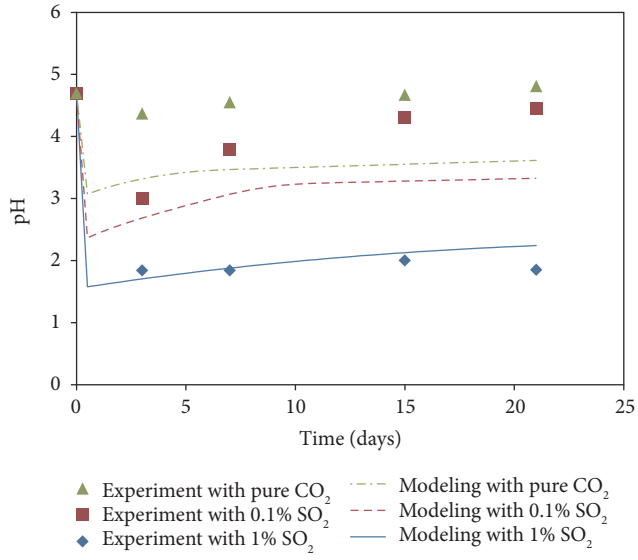

Figure 2: Changes in pH measured during gas-water-rock experiments (green triangle = pure CO_2 case, red square = 0.1% SO_2 case, and blue rhombus = 1% SO_2 case) and changes in pH in the modeling (green dashed line = pure CO_2 case, red dashed line = 0.1% SO_2 case, and blue solid line = 1% SO_2 case).

3. Results and Discussion

3.1. pH. Figure 2 shows the change in pH according to reaction time in this experiment. In all cases, pH decreased at the beginning of the experiment and the more the concentration of SO_2 increased, the more the pH decreased. After 3 days of the experiment, the pH decreased from 4.7 to 4.37 in the pure CO_2 case and to 3 in the 0.1% SO_2 case. In the 1% SO_2 case, the pH significantly decreased to 1.84. In the presence of SO_2, the formation of sulfuric acid increased the number of H^+ ions in the water, thereby reducing the pH more than if reacting with pure CO_2 [15, 33]. This can be supported by the sulfate concentrations measured in the experiments (Figure 3). Sulfate formed by the dissociation of SO_2 initially increased from zero up to 360 ppm and 4500 ppm in the 0.1% SO_2 and 1% SO_2 cases, respectively, after 7 days of the experiment (Figure 3). The increased sulfate concentrations indicate that a large amount of sulfuric acid was formed in the water and consequently caused a significant decrease in the pH. Figure 2 also shows that the pH gradually increased up to 4.45 in the pure CO_2 case and up to 4.81 in the 0.1% SO_2 case at the end of the experiment (after 21 days). In contrast, the pH remained less than 2 in the 1% SO_2 case during the entire experiment.

The geochemical modeling also shows similar results to the experiments (Figure 2). However, the pH of the modeling results was lower than that of the experiments in the pure CO_2 and 0.1% SO_2 cases. This difference in pH between the models and the experiment may have been caused by degassing of CO_2 during sampling in the experiments. In contrast, the pH had no significant difference in the 1% SO_2

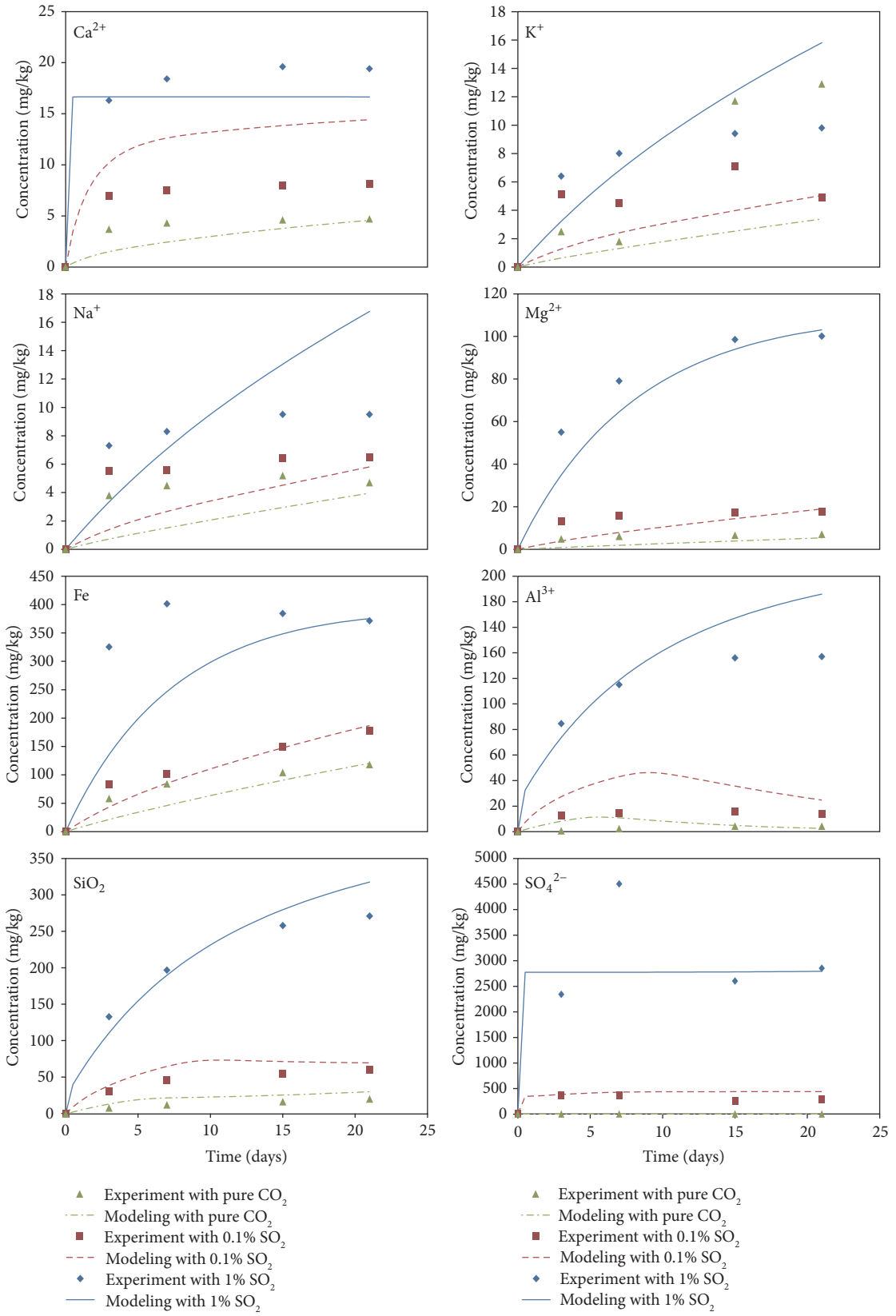

Figure 3: Changes in the concentration of cations during gas-water-rock experiments (green triangle = pure CO_2 case, red square = 0.1% SO_2 case, and blue rhombus = 1% SO_2 case) and changes in the concentration of cations in the modeling (green dashed line = pure CO_2 case, red dashed line = 0.1% SO_2 case, and blue solid line = 1% SO_2 case).

Table 2: Kinetic rate parameters for dissolution/precipitation of minerals used in this study.

	Acid			Neutral		Base		
	$\log K$ (mol/m^2/s)	E_a (kJ/mol)	n	$\log K$ (mol/m^2/s)	E_a (kJ/mol)	$\log K$ (mol/m^2/s)	E_a (kJ/mol)	n
Albite	−10.16	65.00	0.46	−12.56	69.80	−15.60	71.00	−0.570
Anorthite	−3.50	16.60	1.41	−9.12	17.80			
Clinochlore-14A	−11.11	88.00	0.50	−12.52	88.00			
Daphnite-14A	−11.11	88.00	0.50	−12.52	88.00			
Illite	−10.98	23.60	0.340	−12.78	35.00	−16.52	58.90	−0.400
Kaolinite	−11.31	65.90	0.777	−13.18	22.20	−17.05	17.90	−0.472
K-feldspar	−10.06	51.70	0.50	−12.41	38.00	−21.20	94.10	−0.820
Montmorillonite-Mg	−12.71	48.00	0.220	−14.41	48.00	−14.41	48.00	−0.130
Pyrite				−10.40	62.76			
Quartz				−13.40	90.90			

case. The reason for this phenomenon can be explained by the following equations:

$$H_2CO_3 = H^+ + HCO_3^- \quad (5)$$

$$pH = \log \frac{[HCO_3^-]}{[H_2CO_3]} + 6.35. \quad (6)$$

The dissociation of H_2CO_3 is described by (5), and when this formula is log-transformed, the relation between pH and the carbonate species is as shown in (6). The pH is determined by the ratio of HCO_3^- to H_2CO_3 as in (6). In a low pH (pH < 2) environment, carbon species are predominantly present as H_2CO_3 and rarely have HCO_3^-. Thus, the loss of H_2CO_3 by CO_2 degassing cannot significantly change pH.

The gradual increase in the pH of pure CO_2 and 0.1% SO_2 cases can be accounted for by the buffering effect of mineral dissolution with reaction time. In contrast, a very low pH (<2) during the experiments in the 1% SO_2 case shows insufficient buffering capacity. On the other hand, several researchers have shown that even when strong sulfuric acid is formed in solution due to the presence of SO_2, pH can be buffered if carbonate minerals are sufficiently present in the reservoir rocks [6, 15].

Considering the mineral compositions in this study, however, our results indicate that the buffering capacity of the silicate minerals is insufficient to increase pH in the 1% SO_2 case. In a captured CO_2 for geologic storage condition, 1% of SO_2 content is unrealistically high in comparison to practically coinjective SO_2 content. The content of SO_2 contained in captured CO_2 is generally limited to less than 100 ppm [12]. However, the content of SO_2 in a storage aquifer can be increased by accumulating SO_2 locally with a structural trap or mass transfer limit [11, 14]. This implies that if the accumulation of SO_2 occurs in an area of storage aquifers, the pH may maintain a low level due to insufficient buffering capacity. This acidic environment can enhance the dissolution of constituent minerals, which increases the porosity of storage rocks around the CO_2 injection well, whereas it may cause CO_2 leakage through formation of a vertical leakage path in cap rocks [6, 10].

3.2. SO_2-CO_2-Water-Rock Interaction

3.2.1. Ion Concentrations. To evaluate SO_2-CO_2-water-rock interactions, the ion concentrations measured in the experiments and simulated by modeling with reaction time are presented in Figure 3. The changes in the quantities of the minerals calculated by modeling are also shown in Figure 4. As shown in Figure 3, our experimental results show that the increasing concentrations of cations are dependent on the SO_2 contents similar to the changes in pH. Compared to the pure CO_2 case, the concentrations of cations in the 0.1% SO_2 case slightly increase, while those in the 1% SO_2 case significantly increase even at the initial stage of the experiment. This result shows that a higher content of SO_2 leads to enhanced mineral dissolution through formation of an acidified condition. This is because the dissolution of silicate minerals is pH-dependent [29, 34] and our result is also in good agreement with other studies [4, 6, 13, 15, 33]. This is clearly shown by the changes in the quantities of the minerals with time (Figure 4). The dissolution rates of the primary minerals in the 0.1% SO_2 case slightly increase, whereas those of the primary minerals abruptly increase in the 1% SO_2 case because of a very low pH (Figure 4).

The results of the geochemical modeling are also similar to those of the experiments, although there is a discrepancy between measured data and simulated data in each case. This gap may arise from the uncertainties of rate constant, mass fraction of minerals, reactive surface area, and thermodynamic data [35, 36]. Nonetheless, we consider that the modeling results are acceptable considering only dissolution/precipitation of the minerals (Table 3).

3.2.2. Change in Mineralogy. The results of SEM-EDS analysis were shown in Figure 5. Traces of corrosion were observed by dissolution at the surface of minerals. In particular, in the 1% SO_2 case, corrosion was prominent on the surface of feldspar

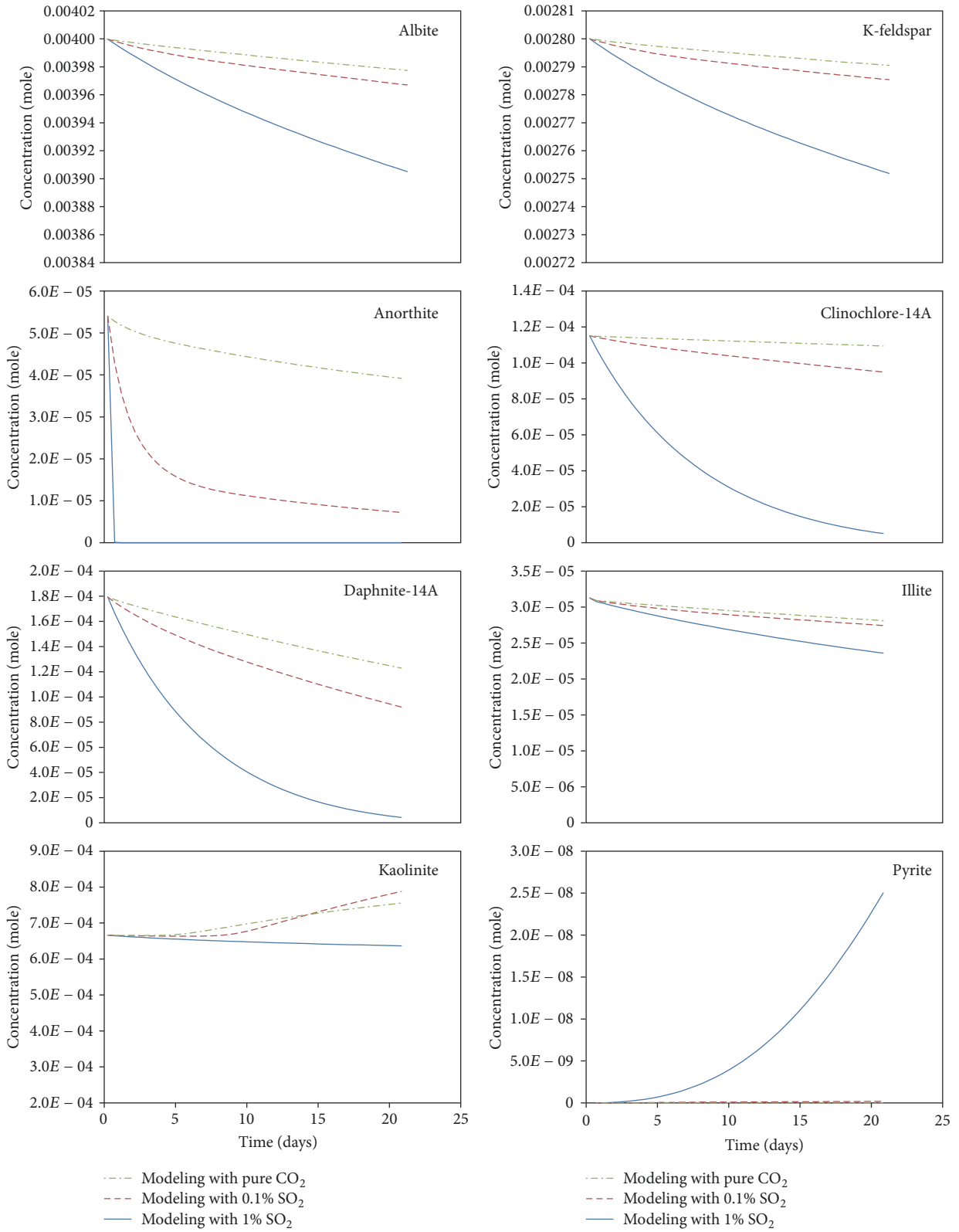

Figure 4: Changes in the concentration of minerals in the modeling (green dashed line = pure CO_2 case, red dashed line = 0.1% SO_2 case, and blue solid line = 1% SO_2 case).

Table 3: Dissolution equations of minerals used in this study.

	Dissolution equations	log K (25°C)
Albite	$NaAlSi_3O_8 + 4H^+ = Al^{3+} + Na + H_2O + 3SiO_2$	2.76
Anorthite	$CaAl_2(SiO_4)_2 + 8H^+ = Ca^{2+} + 2Al^{3+} + 2SiO_2 + 4H_2O$	26.57
Clinochlore-14A	$Mg_5Al_2Si_3O_{10}(OH)_8 + 16H^+ = 2Al^{3+} + 3SiO_2 + 5Mg^{2+} + 12H_2O$	67.23
Daphnite-14A	$Fe_5AlAlSi_3O_{10}(OH)_8 + 16H^+ = 2Al^{3+} + 3SiO_2 + 5Fe^{2+} + 12H_2O$	52.28
Illite	$K_{0.6}Mg_{0.25}Al_{1.8}Al_{0.5}Si_{3.5}O_{10}(OH)_2 + 8H^+ = 0.25Mg^{2+} + 0.6K^+ + 2.3Al^{3+} + 3.5SiO_2 + 5H_2O$	9.02
Kaolinite	$Al_2Si_2O_5(OH)_4 + 6H^+ = 2Al^{3+} + 2SiO_2 + 5H_2O$	6.81
K-feldspar	$KAlSi_3O_8 + 4H^+ = Al^{3+} + K^+ + 2H_2O + 3SiO_2$	−0.27
Montmorillonite-Mg	$Mg_{.495}Al_{1.67}Si_4O_{10}(OH)_2 + 6H^+ = 0.495Mg^{2+} + 1.67Al^{3+} + 4H_2O + 4SiO_2$	2.38
Pyrite	$FeS_2 + H_2O = 0.25H^+ + 0.25SO_4^{2-} + Fe^{2+} + 1.75HS^-$	−24.65
Quartz	$SiO_2 = SiO_2$	−3.99

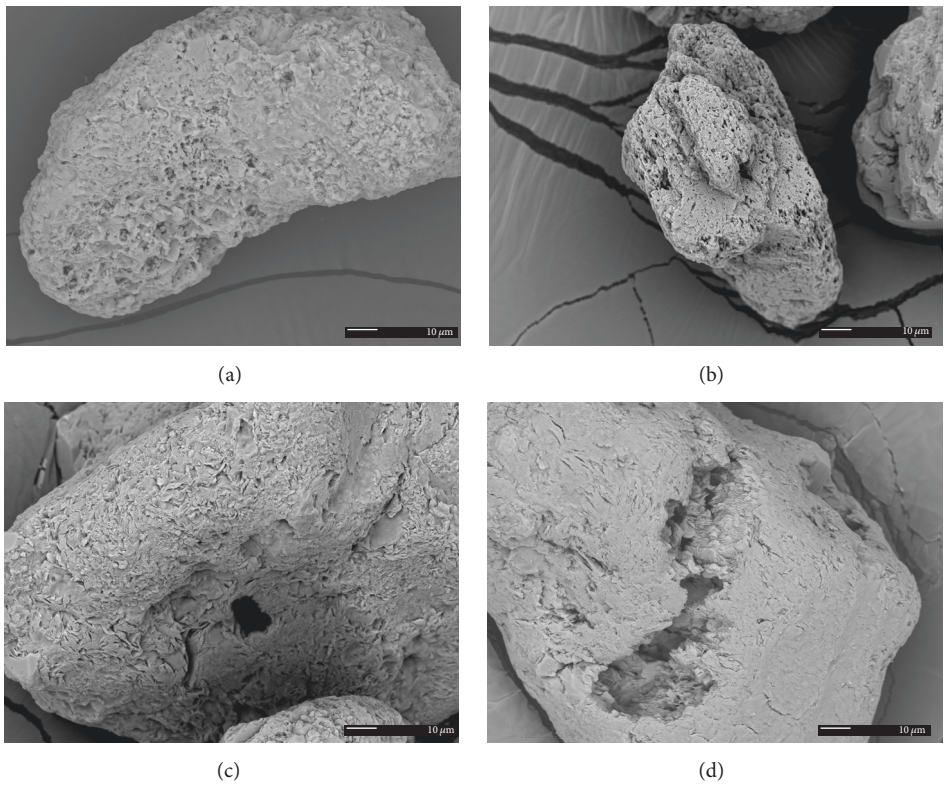

(a) (b) (c) (d)

Figure 5: SEM electron backscatter images of the dissolved mineral surface by SO_2-CO_2-water interaction in the experiments: (a) K-Na plagioclase in 0.1% SO_2 case, (b) Na-plagioclase in 1% SO_2 case, (c) chlorite in 0.1% SO_2 case, and (d) chlorite in 1% SO_2 case.

(Figures 5(a) and 5(b)) and chlorite (Figures 5(c) and 5(d)). On the surface of some chlorite grains, cracks or holes were observed (Figures 5(c) and 5(d)).

The dissolution/precipitation of minerals is shown in Figure 4, and the dissolution equations of the minerals are presented in Table 3. The results of geochemical modeling also supported the fact that the concentrations of most primary minerals decrease by dissolution in all cases. Feldspars (plagioclase and K-feldspar) and chlorite (clinochlore and daphnite) are predominantly dissolved (anorthite will be excluded from discussion because it was added to fit the low concentration of Ca).

Feldspar does not have a faster reaction rate than carbonate minerals, but it contributed to the increase in cations (Na, K, Ca, Si, and Al) because of its high content in the rock. In contrast, chlorite (4.8 wt.% of total minerals) caused the release of a large amount of Fe and Mg. Chlorite plays an important role in the increase in Fe and Mg concentrations in other studies under CO_2-rich conditions [6, 15, 37, 38].

The secondary minerals that newly precipitated following the dissolution of the primary minerals are also shown in Figure 4. In our modeling, kaolinite is distinctly precipitated in the pure CO_2 and 0.1% SO_2 cases because of the dissolution of silicate minerals (Table 3). In the SEM-EDS analysis, a large

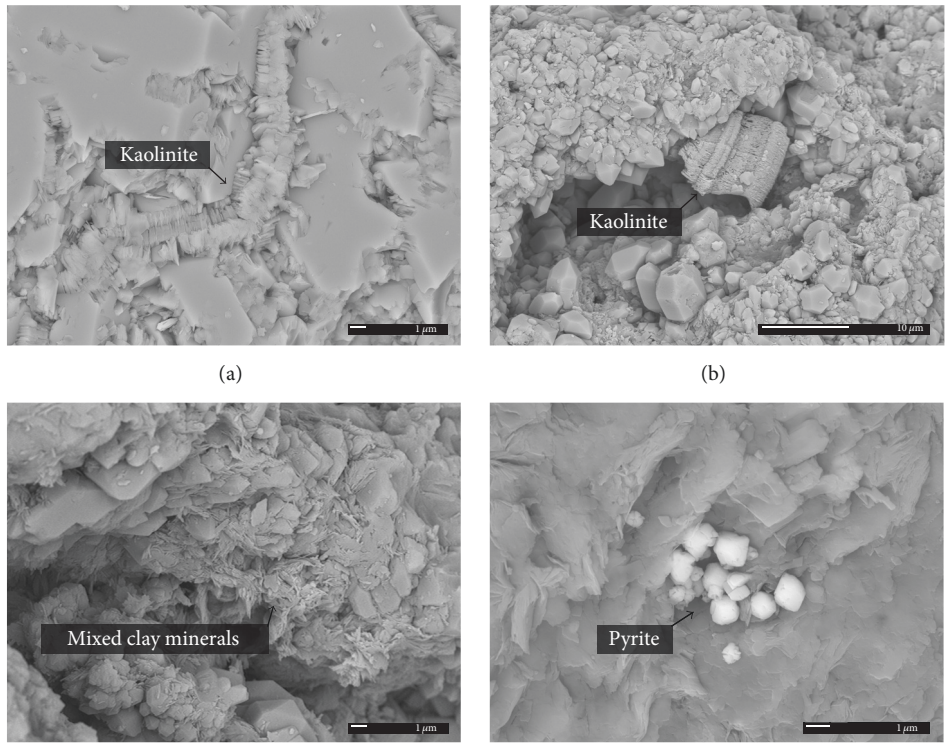

Figure 6: SEM electron backscatter images of precipitated secondary minerals by SO_2-CO_2-water interaction in the experiments: (a) kaolinite in pure CO_2 case, (b) kaolinite in 0.1% SO_2 case, (c) mixed clay minerals in 0.1% SO_2 case, and (d) pyrite in 1% SO_2 case.

Table 4: Calculated mineral saturation indices with reaction time.

	Time (days)	Anhydrite	Alunite	Calcite	Gypsum	Kaolinite	Montmorillonite-Mg	Siderite	Pyrite
1% SO_2	1	−1.66	−7.72	−8.07	−1.74	−8.02	−10.17	−5.57	6.29
	3	−1.63	−5.95	−7.88	−5.95	−6.40	−7.83	−4.97	6.85
	7	−1.59	−4.01	−7.55	−1.68	−4.58	−5.48	−4.39	7.36
	15	−1.55	−1.84	−7.08	−1.64	−2.56	−3.09	−3.77	7.87
	21	−1.54	−0.94	−6.86	−1.62	−1.71	−2.13	−3.52	8.06
0.1% SO_2	1	−2.28	−4.19	−6.67	−2.37	−4.32	−7.82	−4.26	5.37
	3	−2.01	−1.38	−5.96	−2.09	−1.60	−4.28	−3.39	5.82
	7	−1.90	1.72	−5.12	−1.98	1.43	−0.71	−2.43	5.63
	15	−1.85	2.93	−4.67	−1.94	2.58	0.68	−1.84	5.45
	21	−1.83	2.83	−4.56	−1.91	2.51	0.69	−1.66	5.47
Pure CO_2	1	n.d.	n.d.	−6.06	n.d.	−1.64	−6.32	−3.22	n.d.
	3	n.d.	n.d.	−5.38	n.d.	0.99	−2.76	−2.50	n.d.
	7	n.d.	n.d.	−4.89	n.d.	2.45	−0.75	−1.96	n.d.
	15	n.d.	n.d.	−4.54	n.d.	2.38	−0.41	−1.55	n.d.
	21	n.d.	n.d.	−4.34	n.d.	2.29	−0.19	−1.34	n.d.

n.d.: not determined.

amount of kaolinite was easily observed on the surface of the mineral after the experiment in the pure CO_2 and 0.1% SO_2 cases (Figures 6(a) and 6(b)). Saturation indices calculated by measured ion concentrations in the experiments also show that kaolinite is oversaturated during the experiments in the pure CO_2 and 0.1% SO_2 cases (Table 4). However, in this model, kaolinite is not precipitated in the 1% SO_2 case, and the saturation index of kaolinite is undersaturated because of the very low pH (<2) (Figure 4 and Table 4). In the SEM-EDS observation, other clay minerals were also observed but could not be identified to a specific mineral because they were present as mixed clay minerals (Figure 6(c)). However, in the modeling, montmorillonite-Mg is precipitated at the end of the simulation time in the 0.1% SO_2 case (not presented

because of a very small amount of precipitation) and the calculated saturation index of the montmorillonite-Mg is oversaturated at the end of the experiments in the 0.1% SO_2 case (Table 4). This suggests that montmorillonite clays can be newly formed by enhanced water-rock interactions when the pH is greater than 4.

The formation of pyrite has been reported in studies of SO_2-CO_2-water-rock interactions [12, 38]. Pyrite is stable under relatively low pH conditions [39]. In this study, the modeling result also shows the precipitation of pyrite in the 0.1% SO_2 and 1% SO_2 cases, although only a small amount of pyrite was formed (Figure 4) (note that the precipitation of pyrite in the 0.1% SO_2 case is hidden because it is a very small amount). In the SEM-EDS analysis, a small amount of pyrite was observed on the surface of the minerals, although it was difficult to detect (Figure 6(d)). This is due to slow precipitation kinetics in real conditions, although saturation indices for pyrite calculated under thermodynamic equilibrium are highly positive (SI > 5) (Table 4). Nonetheless, this result shows that the coinjection of SO_2 is favorable to the formation of pyrite by consuming Fe^{2+} instead of siderite (Table 4).

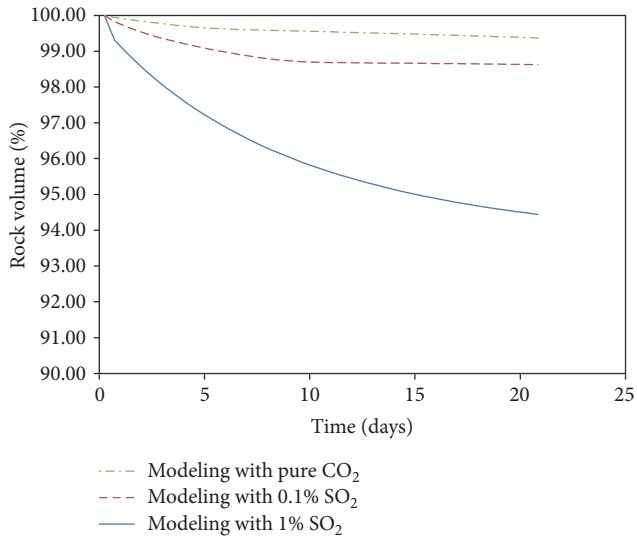

Figure 7: Changes in the volume of total minerals in the modeling (green dashed line = pure CO_2 case, red dashed line = 0.1% SO_2 case, and blue solid line = 1% SO_2 case).

3.2.3. Comparison to Other Studies. Several researchers have reported that sulfate minerals such as gypsum, anhydrite, and alunite are formed by SO_2-CO_2-water-rock interaction when Ca-rich minerals such as calcite and anorthite are present [4, 12, 16, 37]. They also reported that the precipitation of sulfate minerals may be a factor in reducing porosity near injection wells. For example, Waldmann and Rütters [4] investigated the impact of SO_2 on porosity change in the presence of Ca-rich minerals such as carbonate and anorthite. They showed that the dissolution of Ca-rich minerals buffered the pH providing Ca to the groundwater, and then anhydrite was preferentially precipitated. However, in this study, we could not observe in the SEM-EDS analysis and the modeling results during the reaction periods the formation of gypsum or anhydrite which can be formed preferably to calcite by consuming Ca. Calculated saturation indices also showed that all water samples were undersaturated with respect to gypsum and anhydrite (Table 4). This is because the concentration of Ca was not enough to precipitate gypsum or anhydrite due to the absence of Ca-rich minerals (e.g., calcite and anorthite) in this study. Similar result was also observed in a potential CO_2 storage site in the Surat Basin, Australia [12]. In this potential site, Pearce et al. [12] performed laboratory experiments and geochemical modeling for SO_2-CO_2-water-rock reactions using sandstone rocks with no Ca sources (e.g., calcite). Their study showed that gypsum was not precipitated due to low concentrations of dissolved Ca. These results show that Ca-sulfate minerals cannot be precipitated in Ca-deficient condition.

Alunite was also not observed using mineralogical analysis. On the other hand, calculated saturation indices of alunite show an oversaturated state in the 0.1% SO_2 case, whereas they show an undersaturated state in the 1% SO_2 case because of low pH (Table 4). Although it might be possible that a very small quantity of alunite is precipitated in the 0.1% SO_2 case, we could not confirm the formation of alunite because it was not observed in mineralogical analysis. In this study, calcite, which is commonly observed in CO_2-water-rock reactions, was not detected, similar to gypsum or anhydrite for all the experimental cases. The saturation index of calcite was also a negative value (undersaturation) (Table 4). This can be explained by the low concentration of Ca and the low pH caused by the low buffering capacity in this study.

3.3. Porosity Change. To evaluate the impact of SO_2-CO_2-water-rock interactions on the porosity of the reservoir rock, the change in total rock volume was calculated with reaction time using the molar volume of each mineral in the modeling (Figure 7). Pyrite and montmorillonite-Mg were excluded because they had little influence on total rock volume due to their very small quantities. As shown in Figure 7, total rock volume decreased with reaction time for all cases, which means that porosity and permeability in the rock increased. As previously discussed, total rock volume in the 1% SO_2 case significantly decreased because of the enhanced dissolution of minerals.

To identify the contribution of each mineral to the decrease in total rock volume, the volume change of each mineral was calculated at the end of the simulation (Figure 8). As seen in Figure 8, the volumes of most primary minerals (except quartz and kaolinite) decreased due to dissolution. In particular, the dissolution of chlorite (clinochlore-14A and daphnite-14A) showed the largest influence on the decrease in rock volume (Figure 8), although chlorite constituted only 4.8 wt.% of the reservoir rock. On the other hand, the volume of kaolinite increased in the pure CO_2 and 0.1% SO_2 cases due to precipitation. According to Pearce et al. [15], the precipitation of kaolinite has the potential to reduce porosity and permeability not only in the reaction with pure CO_2 but also in the reaction with SO_2-CO_2. In our study, the increased volume of kaolinite by precipitation could not compensate for

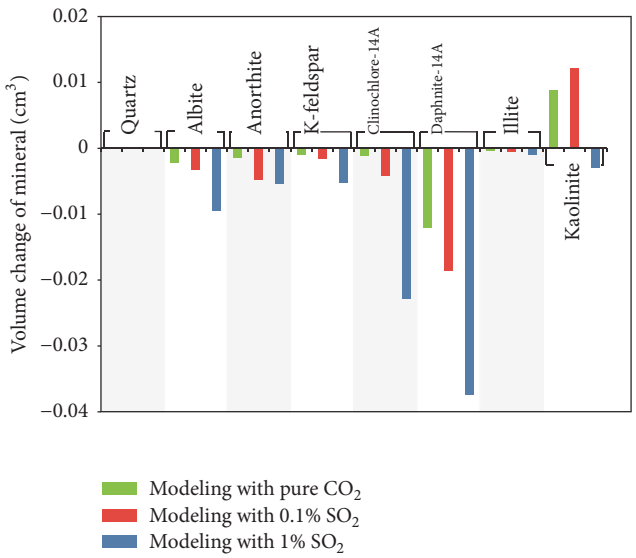

Figure 8: Changes in the volume of primary minerals in the modeling (green bar = pure CO_2 case, red bar = 0.1% SO_2 case, and blue bar = 1% SO_2 case).

the loss of total rock volume by dissolution (Figure 8); total rock volume decreased.

The dissolution of mineral also may affect the integrity and the mechanical properties of reservoir rocks [4, 40–43]. This dissolution reaction by CO_2-water-reservoir rock interaction includes relatively rapid dissolution of fast-reacting minerals such as carbonates, present either as framework grains or as intergranular cement [41, 42]. The rocks with high carbonate content such as carbonate reservoir are relatively prone to mechanical weakening due to dissolution of carbonate minerals [43]. In addition, in the sandstone reservoir, mechanical properties of rocks are locally affected by dissolution of carbonate cements between the grains [4, 40]. According to Hangx et al. [42], however, rock mechanical properties were not affected because the framework grains were sufficiently quartz-cemented, although small amount of calcite was completely dissolved in a sandstone; no shear failure of a reservoir is expected during CO_2 injection. They also said that long-term effect of aluminosilicate reactions on mechanical properties requires further research but it is out of scope of this study.

From our results, this study shows that SO_2-CO_2-water-rock interactions within a reservoir with Ca-deficient conditions and poor buffering capacity can significantly increase the porosity of the reservoir rock, unlike results of other studies [4, 16, 21]. Those studies showed that sulfate minerals such as anhydrate, gypsum, and alunite are precipitated by reacting with SO_2 when Ca-rich minerals such as calcite and anorthite are present, which decreases the porosity of the rocks.

4. Conclusions

This study was conducted to evaluate the effect of SO_2 on water-rock interactions in a reservoir rock having Ca-deficient conditions and poor buffering capacity and to evaluate the change in porosity affecting CO_2 injectivity. Our results show that SO_2 significantly lowered pH and that a strong acidic condition was maintained during the experiments when buffering capacity was insufficient. This accelerated the dissolution of the primary minerals, and thus the total volume of the reservoir rock decreased. The dissolution of chlorite was mainly responsible for the decrease in total rock volume. The newly formed secondary minerals varied according to the mixed gases: pure CO_2 (kaolinite), 0.1% SO_2 (kaolinite, montmorillonite-Mg, and pyrite), and 1% SO_2 (pyrite). However, sulfate minerals (gypsum or anhydrite) were not formed due to an insufficient supply of Ca. Thus, in this study, the total volume of precipitated secondary minerals could not compensate for the loss in total rock volume, which indicates that porosity in the reservoir rock increased.

This study indicates that a certain amount of SO_2 coinjection with CO_2 in a rock having no carbonate or Ca-rich minerals may be more beneficial to the injection because of a porosity increase resulting from SO_2-CO_2-water-rock interaction.

Conflicts of Interest

The authors declare that there are no conflicts of interest regarding the publication of this paper.

Acknowledgments

This study was supported by the Basic Research Program (GP2017-027) of the Korea Institute of Geoscience and Mineral Resources (KIGAM) and by the Korea Institute of Energy Technology Evaluation and Planning (KETEP) grant funded by the Ministry of Trade, Industry & Energy, Korean Government (no. 20162010201980).

References

[1] IPCC., "Special Report on carbon dioxide capture and storage," in *Prepared by Working Group III of the Intergovernmental Panel on Climate Change*, B. Metz, O. Davidson, H. de Coninck, M. Loos, and L. Meyer, Eds., p. 442, Cambridge University Press, Cambridge, United Kingdom, 2005.

[2] S. Bachu, "CO_2 storage in geological media: role, means, status and barriers to deployment," *Progress in Energy and Combustion Science*, vol. 34, no. 2, pp. 254–273, 2008.

[3] A. Kather and S. Kownatzki, "Assessment of the different parameters affecting the CO_2 purity from coal fired oxyfuel process," *International Journal of Greenhouse Gas Control*, vol. 5, no. 1, pp. S204–S209, 2011.

[4] S. Waldmann and H. Rütters, "Geochemical effects of SO_2 during CO_2 storage in deep saline reservoir sandstones of Permian age (Rotliegend) - a modeling approach," *International Journal of Greenhouse Gas Control*, vol. 46, pp. 116–135, 2016.

[5] J. Wang, Z. Wang, D. Ryan, and C. Lan, "A study of the effect of impurities on CO_2 storage capacity in geological formations," *International Journal of Greenhouse Gas Control*, vol. 42, pp. 132–137, 2015.

[6] T. Xu, J. A. Apps, K. Pruess, and H. Yamamoto, "Numerical modeling of injection and mineral trapping of CO_2 with H_2S

and SO_2 in a sandstone formation," *Chemical Geology*, vol. 242, no. 3-4, pp. 319–346, 2007.

[7] K. G. Knauss, J. W. Johnson, and C. I. Steefel, "Evaluation of the impact of CO_2, co-contaminant gas, aqueous fluid and reservoir rock interactions on the geologic sequestration of CO2," *Chemical Geology*, vol. 217, no. 3-4, pp. 339–350, 2005.

[8] J. Wang, D. Ryan, E. J. Anthony, N. Wildgust, and T. Aiken, "Effects of impurities on CO_2 transport, injection and storage," *Energy Procedia*, vol. 4, pp. 3071–3078, 2011.

[9] J. P. Kaszuba, D. R. Janecky, and M. G. Snow, "Experimental evaluation of mixed fluid reactions between supercritical carbon dioxide and NaCl brine: relevance to the integrity of a geologic carbon repository," *Chemical Geology*, vol. 217, no. 3-4, pp. 277–293, 2005.

[10] L. E. Crandell, B. R. Ellis, and C. A. Peters, "Dissolution potential of SO_2 co-injected with CO_2 in geologic sequestration," *Environmental Science & Technology*, vol. 44, no. 1, pp. 349–355, 2010.

[11] B. R. Ellis, L. E. Crandell, and C. A. Peters, "Limitations for brine acidification due to SO_2 co-injection in geologic carbon sequestration," *International Journal of Greenhouse Gas Control*, vol. 4, no. 3, pp. 575–582, 2010.

[12] J. K. Pearce, D. M. Kirste, G. K. W. Dawson et al., "SO_2 impurity impacts on experimental and simulated CO_2-water-reservoir rock reactions at carbon storage conditions," *Chemical Geology*, vol. 399, pp. 65–86, 2015.

[13] G. K. W. Dawson, J. K. Pearce, D. Biddle, and S. D. Golding, "Experimental mineral dissolution in Berea Sandstone reacted with CO_2 or SO_2-CO_2 in NaCl brine under CO_2 sequestration conditions," *Chemical Geology*, vol. 399, pp. 87–97, 2015.

[14] M. Koenen, T. J. Tambach, and F. P. Neele, "Geochemical effects of impurities in CO_2 on a sandstone reservoir," *Energy Procedia*, vol. 4, pp. 5343–5349, 2011.

[15] J. K. Pearce, A. Golab, G. K. W. Dawson, L. Knuefing, C. Goodwin, and S. D. Golding, "Mineralogical controls on porosity and water chemistry during O_2-SO_2-CO_2 reaction of CO_2 storage reservoir and cap-rock core," *Applied Geochemistry*, vol. 75, pp. 152–168, 2016.

[16] S. Renard, J. Sterpenich, J. Pironon, P. Chiquet, and A. Randi, "Geochemical effects of an oxycombustion stream containing SO_2 and O_2 on carbonate rocks in the context of CO_2 storage," *Chemical Geology*, vol. 382, pp. 140–152, 2014.

[17] B.-Y. Choi, Y.-J. Shinn, Y.-C. Park, J. Park, Y.-K. Kwon, and K.-Y. Kim, "Simulation of CO_2 injection in a small-scale pilot site in the Pohang Basin, Korea: effect of dissolution rate of chlorite on mineral trapping," *International Journal of Greenhouse Gas Control*, vol. 59, pp. 1–12, 2017.

[18] J. C. Ingle Jr., "Subsidence of the Japan Sea: stratigraphic evidence from ODP site and onshore section," *Proceedings of the ODP Sci. Result, 127/128*, pp. 119–1212, 1992.

[19] S. H. Yoon and S. K. Chough, "Regional strike slip in the eastern continental margin of Korea and its tectonic implications for the evolution of Ulleung Basin, East Sea (Sea of Japan)," *Geological Society of America Bulletin*, vol. 107, no. 1, pp. 83–97, 1995.

[20] Y. K. Sohn and M. Son, "Synrift stratigraphic geometry in a transfer zone coarse-grained delta complex, Miocene Pohang Basin, SE Korea," *Sedimentology*, vol. 51, no. 6, pp. 1387–1408, 2004.

[21] Y. Cheon, M. Son, C. W. Song, J.-S. Kim, and Y. K. Sohn, "Geometry and kinematics of the Ocheon Fault System along the boundary between the Miocene Pohang and Janggi basins, SE Korea, and its tectonic implications," *Geosciences Journal*, vol. 16, no. 3, pp. 253–273, 2012.

[22] I. G. Hwang and S. K. Chough, "The Maesan fan delta, Miocene Pohang Basin, SE Korea: Architecture and depositional processes of a high-gradient fan-delta-fed slope system," *Sedimentology*, vol. 47, no. 5, pp. 995–1010, 2000.

[23] Y. K. Sohn, C. W. Rhee, and H. Shon, "Revised stratigraphy and reinterpretation of the Miocene Pohang basinfill, SE Korea: sequence development in response to tectonism and eustasy in a back-arc basin margin," *Sedimentary Geology*, vol. 143, no. 3-4, pp. 265–285, 2001.

[24] H. Lee, Y. J. Shinn, S. H. Ong et al., "Fault reactivation potential of an offshore CO_2 storage site, Pohang Basin, South Korea," *Journal of Petroleum Science and Engineering*, vol. 152, pp. 427–442, 2017.

[25] M. M. Allan, A. Turner, and B. W. D. Yardley, "Relation between the dissolution rates of single minerals and reservoir rocks in acidified pore waters," *Applied Geochemistry*, vol. 26, no. 8, pp. 1289–1301, 2011.

[26] J. K. Pearce, A. C. K. Law, G. K. W. Dawson, and S. D. Golding, "SO_2-CO_2 and pure CO_2 reactivity of ferroan carbonates at carbon storage conditions," *Chemical Geology*, vol. 411, pp. 112–124, 2015.

[27] D. L. Parkhurst and C. A. J. Appelo, "Description of input and examples for PHREEQC version 3-a computer program for speciation, batch-reaction, one-dimensional transport, and inverse geochemical calculationst," *U. S. Geological Survey, Techniques and Methods 6-A43*, 2013.

[28] A. C. Lasaga, *Kinetic Theory in the Earth Sciences*, Princeton University Press, Princeton, NJ, USA, 1998.

[29] A. C. Lasaga, "Fundamental approaches in describing mineral dissolution and precipitation rates," *Reviews in Mineralogy and Geochemistry*, vol. 31, pp. 23–86, 1995.

[30] S. Amin, D. J. Weiss, and M. J. Blunt, "Reactive transport modelling of geologic CO_2 sequestration in saline aquifers: The influence of pure CO_2 and of mixtures of CO_2 with CH_4 on the sealing capacity of cap rock at 37∘C and 100bar," *Chemical Geology*, vol. 367, pp. 39–50, 2014.

[31] J. L. Palandri and Y. K. Kharaka, "A compilation of rate parameters of water-mineral interaction kinetics for application to geochemical modeling," *Open File Report, U. S. Geological Survey*, 2004.

[32] T. Xu, J. A. Apps, and K. Pruess, "Mineral sequestration of carbon dioxide in a sandstone-shale system," *Chemical Geology*, vol. 217, no. 3-4, pp. 295–318, 2005.

[33] P. Bolourinejad and R. Herber, "Chemical effects of sulfur dioxide co-injection with carbon dioxide on the reservoir and caprock mineralogy and permeability in depleted gas fields," *Applied Geochemistry*, vol. 59, pp. 11–22, 2015.

[34] S. L. Brantley, "Kinetics of mineral dissolution," *Kinetics of Water-Rock Interaction*, pp. 151–210, 2008.

[35] F. Gherardi, T. Xu, and K. Pruess, "Numerical modeling of self-limiting and self-enhancing caprock alteration induced by CO_2 storage in a depleted gas reservoir," *Chemical Geology*, vol. 244, no. 1-2, pp. 103–129, 2007.

[36] S. A. Carroll, W. W. McNab, Z. Dai, and S. C. Torres, "Reactivity of Mount Simon sandstone and the Eau Claire shale under CO_2 storage conditions," *Environmental Science & Technology*, vol. 47, no. 1, pp. 252–261, 2013.

[37] S. M. Farquhar, J. K. Pearce, G. K. W. Dawson et al., "A fresh approach to investigating CO_2 storage: Experimental CO_2-water-rock interactions in a low-salinity reservoir system," *Chemical Geology*, vol. 399, pp. 98–122, 2015.

[38] C. Li, F. Zhang, C. Lyu, J. Hao, J. Song, and S. Zhang, "Effects of H_2S injection on the CO_2-brine-sandstone interaction under 21 MPa and 70 ∘C," *Marine Pollution Bulletin*, vol. 106, no. 1-2, pp. 17–24, 2016.

[39] W. Zhang, T. Xu, and Y. Li, "Modeling of fate and transport of coinjection of H_2S with CO_2 in deep saline formations," *Journal of Geophysical Research: Atmospheres*, vol. 116, no. B2, 2011.

[40] H. Pape, C. Clauser, J. Iffland, R. Krug, and R. Wagner, "Anhydrite cementation and compaction in geothermal reservoirs: Interaction of pore-space structure with flow, transport, P-T conditions, and chemical reactions," *International Journal of Rock Mechanics and Mining Sciences*, vol. 42, no. 7-8, pp. 1056–1069, 2005.

[41] E. Liteanu, A. Niemeijer, C. J. Spiers, C. J. Peach, and J. H. P. De Bresser, "The effect of CO_2 on creep of wet calcite aggregates," *Journal of Geophysical Research: Solid Earth*, vol. 117, no. 3, Article ID B03211, 2012.

[42] S. Hangx, A. van der Linden, F. Marcelis, and A. Bauer, "The effect of CO_2 on the mechanical properties of the Captain Sandstone: Geological storage of CO_2 at the Goldeneye field (UK)," *International Journal of Greenhouse Gas Control*, vol. 19, pp. 609–619, 2013.

[43] M. M. Alam, M. L. Hjuler, H. F. Christensen, and I. L. Fabricius, "Impact of supercritical CO_2 injection on petrophysical and rock mechanics properties of chalk: an experimental study on chalk from South Arne field, North Sea," in *Proceedings of the SPE Annual Technical Conference and Exhibition*, Denver, Colo, USA.